ISSN 0031-918X, The Physics of Metals and Metallography, 2016, Vol. 117, No. 10, pp. 1038–1046. © Pleiades Publishing, Ltd., 2016.
Original Russian Text © T.I. Nazarova, V.M. Imaev, R.M. Imaev, R.R. Mulyukov, 2016, published in Fizika Metallov i Metallovedenie, 2016, Vol. 117, No. 10, pp. 1073–1081.

STRENGTH AND PLASTICITY

Improvement of Mechanical Properties of the Ti–45Al–5Nb–1Mo–0.2B (at %) Intermetallic Alloy by Means of Microstructure Controlling

T. I. Nazarova*, V. M. Imaev, R. M. Imaev, and R. R. Mulyukov

Institute for Metals Superplasticity Problems, Russian Academy of Sciences, ul. S. Khalturina 39, Ufa, 450001 Russia
**e-mail: nazarova.ti@mail.ru*

Received October 2, 2015; in final form, February 5, 2016

Abstract—The effect of heat and thermomechanical treatments conditions on the microstructure and main mechanical characteristics (obtained by tensile, high-temperature long-term strength, fracture toughness, and high-cycle fatigue tests) of the Ti–45Al–5Nb–1Mo–0.2B (at %) alloy was studied. Before the treatments, the sequence of phase transformations in the alloy after its solidification was determined by test-quenching method. The obtained data were used to develop conditions for the heat and thermomechanical treatments. It was found that a small but stable increase in the plasticity and strength of the cast alloy is observed after three-stage annealing at temperatures that correspond to the ($\alpha + \gamma$)- and ($\alpha_2 + \beta(B2) + \gamma$)-phase region. The thermomechanical treatment at temperatures corresponding to the ($\alpha(\alpha_2) + \beta(B2) + \gamma$)-phase region and subsequent two-stage annealing at temperatures that correspond to the ($\alpha + \beta(B2) + \gamma$)- and ($\alpha_2 + \beta(B2) + \gamma$)-phase region lead to the formation of fine-grained duplex structure. This determined the substantial improvement of the low-temperature plasticity and strength ($\delta = 3.1\%$ and $\sigma_u = 860$ MPa at 20°C, respectively) and retained high creep resistance to 700°C.

Keywords: intermetallic γ(TiAl) alloys, microstructure, heat treatment (HT), thermomechanical treatment (TMT), mechanical properties

DOI: 10.1134/S0031918X16080111

INTRODUCTION

At present, light heat-resistant intermetallic alloys based on the γ(TiAl) and $\alpha_2(Ti_3Al)$ phases (from here on, γ(TiAl) alloys) are considered to be a possible structural material for designing an advanced aeroengine characterized by a higher thrust-to-weight ratio [1–5]. The alloys exhibit high specific strength, stiffness, heat resistance, high-temperature strength, and combustion resistance at temperatures of 600–800°C. The specific modulus of elasticity of the γ(TiAl) alloys is 50–70% higher than that of titanium and nickel alloys; the difference remains at high temperatures. The specific strength of γ(TiAl) alloys (with the appropriate microstructure) at temperatures of 600–800°C exceed that of all traditional structural materials [6]. The γ(TiAl) alloys are assumed to be partially substituted for heat-resistant nickel alloys for gas-turbine engines. This will allow one to substantially increase the specific engine performance and simultaneously decrease the fuel consumption, carbon dioxide emission, and engine noisiness.

Difficulties related to the realization of optimum combination of mechanical properties, such as the high heat-resistance, strength, high-temperature strength, and adequate plasticity and fracture toughness hinder the wide application of the γ(TiAl) alloys. It is known that, from the viewpoint of microstructure, the coarse lamellar ($\gamma + \alpha_2$) structure favors reaching high heat resistance and adequate fracture toughness due to the existence of coarse-grained colonies ($d \sim 100$–1000 μm) and coherent and semicoherent γ/γ, γ/α_2 interfaces in them; however, coarse colonies are unfavorable for plastic deformation. γ(TiAl) alloys with the cast coarse lamellar structure exhibit zero plasticity at room temperature. The increase in the plasticity (with elongation by 2–3% or more) of the γ(TiAl) alloys is reached in the cases of duplex and equiaxed fine-grained structures, which are formed by thermomechanical treatment; however, these states are characterized by low heat-resistance and fracture toughness. Due to the fact that the lamellar structure is unstable because of the low α_2-phase content, the duplex structure in the Ti–(47–48)Al–2(Cr or Mn)–2Nb (at %) alloys developed by General Electric in 1986 can be formed by heat treatment, which ensures the plasticity to be at a level of the 1–2% elongation of the alloy at room temperature. This has determined the development of preparation technology of the alloy [7–9]. However, the specific strength of these alloys is lower than that of nickel alloys, and the max-

Table 1. Properties of γ(TiAl) alloys at room temperature

Alloy composition, at %	Structure (treatment)	δ (20°C), %/σ_u (20°C), MPa	T_{max}, °C
Cast alloys			
Ti–48Al–2Cr–2Nb [7]	Duplex (HT)	1.5/476	650–700
Ti–43.7Al–3.2(Nb, Cr, Mo)–0.2B [15]	Fine lamellar (HT)	1.05/630	700–750
Ti–43.5Al–4Nb–1Mo–0.1B [16]	Fine lamellar (HT)	1.16/784	750
Ti–45Al–5Nb–1Mo–0.2B [17]	Fine lamellar (HT)	0.8/670	750
Ti–46Al–8Ta [18]	Fine convolute* (HT)	0.5–1.1/642–666	750–800
Ti–44Al–4Nb–4Hf–0.1Si–0.1B [19]	Lamellar (HT)	0.43/689	750–800
Ti–44Al–8Nb–1B [20]	Fine lamellar (HT)	0.6/699	750–800
Ti–43Al–6Nb–1B [21]	Fine lamellar (HT)	0.4/670	750
Deformed alloys			
Ti–44.2Al–3(Nb, Cr, B) [22]	Fine lamellar (two-stage forging + HT)	2.7/764	700–750
Ti–(46–48)Al–2Cr–2Nb–0.15B [23]	Fine lamellar (extrusion at $T > T_\alpha$ + HT)	3.9–4.7/844–1010**	700
Ti–43.5Al–4Nb–1Mo–0.1B [6]	Duplex (extrusion + single-stage forging + HT)	1–2.2/800–950	700–750
Ti–45Al–5Nb–0.2C–0.2B [24]	Duplex (extrusion + HT)	2.5/1085**	700–750
Ti–(40–44)Al–8.5Nb [25]	Duplex (extrusion + HT)	2.5/≈1000**	700–750
Ti–45Al–8Nb–0.2C [15]	Fine-grained (extrusion + HT)	2.2/910**	700–750
Ti–43Al–6Nb–1B [21]	Duplex (three-stage forging + HT)	2.4/820	750
Ti–44.5Al–6.25Nb–0.8Mo–0.1B [26]	Duplex (single-stage forging + HT)	1.5/800	700–750

* A kind of lamellar structure formed via the massive $\alpha \rightarrow \gamma_{mas}$ transformation.
** Properties were given for the extrusion direction.

imum operating temperature does not exceed 650–700°C. Thus, on the one hand, the low-temperature plasticity and, on the other hand, heat-resistance/strength are inversely dependent on each other, which makes it difficult to achieve the optimum mechanical properties of the γ(TiAl) alloys.

The search for γ(TiAl) alloys characterized by higher heat resistance and strength resulted in the development of so-called TNB and TNM alloys [6, 10–14]. These alloys are characterized by a low aluminum content (usually 43–45 at %) and high contents of alloying elements, and demonstrate substantially higher strength and heat resistance and lower plasticity (in the cast heat-treated state) compared to those of Ti–48Al–2Cr–2Nb alloys.

Table 1 shows the properties of cast and deformed γ(TiAl) alloys at room temperature. It can be seen that the increase in the content of alloying elements and decrease in the aluminum content substantially affect the strength and plasticity parameters of the alloys with comparable structures. Table 1 indicates the maximum operating temperature that increases when the duplex structure changes the lamellar structure and the contents of alloying elements, such as niobium and tantalum increase. The maximum operating temperature of cast heat-treated TNB, TNM, and other γ(TiAl) alloys, which are relatively high-alloyed, exceeds that of the Ti–48Al–2Cr–2Nb alloy by 100°C or more; the specific strength is about 1.4 times higher and the plasticity is slightly lower.

The use of hot deformation allows one to increase the plasticity and strength of alloys; this is accompanied by a slight decrease in the heat resistance. This fact is explained by changes in the structure morphology and colonies/grains refining (Table 1). It should be noted that the high heat resistance of TNB alloys, such as Ti–45Al–8Nb–0.2C, can also remain in a fine-grained state [15, 24, 25] due to the high niobium content and carbon additions that increase the creep resistance. At the same time, the hot extrusion of TNB alloys can result in inhomogeneities in the microstructure, which are due to the chemical microinhomogeneity of the starting cast material and are difficult to eliminate, even after additional thermomechanical treatment [24, 27], and the high niobium content can lead to the formation of brittle ω phase [19, 20, 26]. When considering the mechanical properties of

deformed γ(TiAl) alloys, the high cost and labor intensiveness of deformation processing, which are due to the low manufacturing plasticity of the γ(TiAl) alloys and necessary application of high deformation temperatures (during extrusion, the temperatures are 1250–1400°C) and expensive die materials and consumables, should be taken into account.

The aim of the present study is to achieve the optimum combination of mechanical properties of the γ(TiAl) alloy by heat treatment and technologically uncomplicated thermomechanical processing. The following considerations were taken into account in deciding the composition of the γ(TiAl) alloy: (1) the initial cast alloy should have a structure with small γ/α_2 colonies ($d < 100$ μm), i.e., the alloy should be of those that undergo solidification through the β phase [6, 13, 14]; (2) it is desirable that phase transformations in the alloy can be used to vary the parameters of the microstructure [13, 28]; and (3) the alloy should be moderately alloyed in order for no additional unfavorable phases to be formed or for them to be dissolved. Taking into account the aforementioned considerations, we use the Ti–45Al–5Nb–1Mo–0.2B (at %) alloy as the starting material; it is among TNM alloys (described in detail in [6, 13, 14]) and solidifies through the β phase. This study continues previous works [17].

EXPERIMENTAL

The Ti–45Al–5Nb–1Mo–0.2B (at %) alloy was prepared by GfE Metalle und Materialien GmbH (Germany) and delivered in the form of a rod 120 mm in diameter and 180 mm long. An ingot was prepared by vacuum arc melting and subsequently subjected to mechanical treatment. To determine the phase composition and temperatures of phase transformations, a test-quenching method was used. In this case, samples about 1 cm^3 in volume, which were cut from the ingot, were heated to 900–1350°C, held for 2 h, and subjected to water-quenching. The phase composition of quenched samples was determined by X-ray diffraction analysis and scanning electron microscopy. The temperatures of phase transformations were estimated by differential scanning calorimetry using an STA 449 F1 Jupiter (Netzsch) set up. Heat treatments of samples were performed in air using furnaces manufactured by the Applied Test Systems company.

A blank for the thermomechanical treatment was cut from an ingot. The treatment includes quasi-thermal deformation at temperatures that correspond to the (α(α_2) + β(*B*2) + γ) phase region and the maximum β(*B*2)-phase content. For this purpose, a blank was placed into a carbon-steel envelope, heated to a temperature slightly above the eutectoid transformation temperature, quickly transferred into a die unit heated to 950°C, and subjected to compression at a rate of $\varepsilon' \sim 10^{-2}$–$10^{-1}$ s^{-1} with a degree of deformation of $\varepsilon \approx 70\%$. The deformation was performed using a hydraulic press and a maximum force of 16000 kN. The deformed alloy was drawn out from the envelope and cut into pieces that further were subjected to different heat treatments.

Microstructural studies were performed using a Mira-3 Tescan electron microscope and backscattered electron (BSE) mode that ensures the phase contrast. The average grain (colony) size was determined by random secant method. The volume fraction of the bright β(*B*2) phase was determined by Glagolev's point-counting method. The thickness of plates was measured using transmission electron microscopy. X-ray diffraction analysis was performed using a DRON-4 diffractometer and Co *K*α radiation. To identify reflections and process data, X'Pert HighScore Plus software was used.

Short-term tensile tests were carried out in air at room and high temperatures at the initial deformation rate $\dot{\varepsilon} = 8.3 \times 10^{-4}$ s^{-1}. The tests were performed using planar samples 10 × 5 × 2 mm in gage size, which were spark-cut and mechanically polished. The failure toughness was studied at room temperature at a rate of deformation of 0.5 mm/min by three-point bending tests. In this case, rectangular chevron-notched samples 4.5 × 5.5 × 32 mm in size were used. Long-term strength tests were performed at temperatures of 600, 700, and 750°C for 100 h under loads P = 300–550 MPa using conventional samples 5 mm in gage diameter and 25 mm in gage length. High-cycle fatigue tests were carried out at room temperature at the cycle number $N = 10^7$ and a frequency of 20 Hz using conventional samples. The maximum tensile load was P_{max} = 350 and 400 MPa; the minimum load was P_{min} = 70–80 MPa.

RESULTS AND DISCUSSION

Initial State

Figure 1 shows the macro- and microstructure of the Ti–45Al–5Nb–1Mo–0.2B ingot in the initial cast state. The macrostructure is uniform, lusterless (Fig. 1a); the microstructure consists of nonequiaxed colonies of alternating γ- and α_2-phase plates and interlayers and grains of comparatively dark γ and bright β(*B*2) phases located mainly at colony boundaries (Fig. 1b) (*B*2 is the ordered β-phase modification). The average colony size is $d = 60 \pm 3$ μm. Interlayers and grains of γ- and β(*B*2) phases are mainly elongated in shape and 3–10 μm in width and up to 40 μm long. The volume fraction of the β(*B*2) in the cast alloy is ~5%. The microstructure of ingot demonstrates the presence also of filamentous boride (mono- and diboride [28, 29]) inclusions. The presence of three phases, namely, γ, α_2, and β(*B*2) in the alloy was confirmed by X-ray diffraction analysis data (Fig. 2).

To determine the phase composition and phase-transformation temperatures, alloy samples were

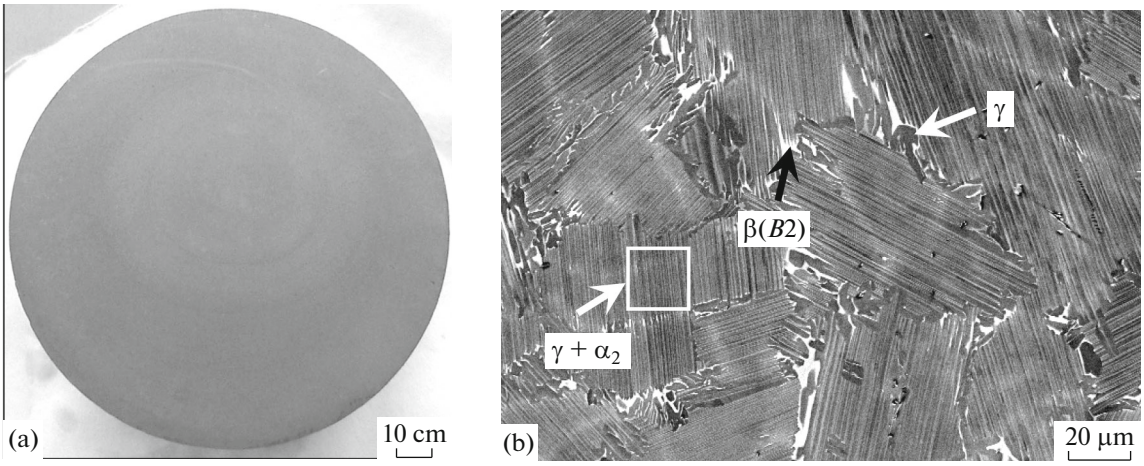

Fig. 1. (a) Macro- and (b) microstructure of the initial cast Ti–45Al–5Nb–1Mo–0.2B alloy (backscattered electron mode).

quenched, and the dependence of the volume fraction of the β(*B*2) phase on the quenching temperature was plotted (Fig. 3). It can be seen that the β(*B*2) phase is present in the alloy in the temperature range 900°C ≤ T < 1300°C; the maximum volume fraction equal to 13 vol % corresponds to a temperature of 1200°C. Based on the results of test quenching and metallographic analysis and taking into account a calculated quasibinary Ti–*x*Al–4Nb–1Mo–0.1B phase diagram previously obtained in [14, 16], the sequence of phase regions during the solidification and cooling of Ti–45Al–5Nb–1Mo–0.2B alloy can be as follows:

$$\mathrm{L} \to \mathrm{L} + \beta \to \beta \to \alpha + \beta \to \alpha \to \alpha + \gamma \to \alpha + \beta(B2) + \gamma \to \alpha + \alpha_2 + \beta(B2) + \gamma \to \alpha_2 + \beta(B2) + \gamma.$$

The temperatures of main phase transitions for the Ti–45Al–5Nb–1Mo–0.2B alloy are T_e = 1189°C, which is the eutectoid transformation temperature; T_α = 1316°C corresponds to the transition to the single-phase α region; and $T_{\alpha \to \alpha + \beta}$ = 1360°C, which is the temperature of the onset of the α → α + β transformation [17].

The conditions of the heat and thermomechanical treatments of the alloy were determined with taking into account the obtained data. The treatment of the alloy was aimed at the following:

(1) refining the microstructure;

(2) the preparation of mainly a lamellar microstructure with equiaxed colonies using heat treatment;

(3) the preparation of a duplex microstructure that contains lamellar and globular components using heat and thermomechanical treatments;

(4) achieving a relatively large distance between lamellae, which is important in order to achieve low-temperature plasticity [17];

(5) the dissolution of the β(*B*2) because it decreases the high-temperature properties of the alloy.

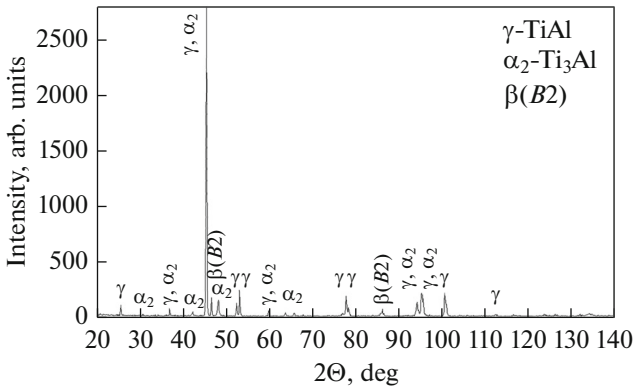

Fig. 2. X-ray diffraction pattern of the Ti–45Al–5Nb–1Mo–0.2B alloy in the initial cast state.

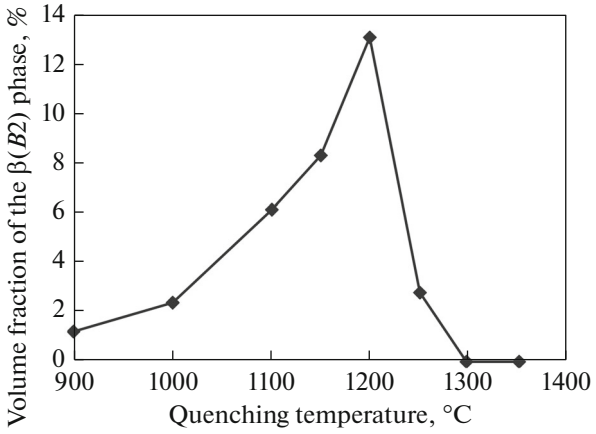

Fig. 3. Dependence of the volume fraction of the β(*B*2) phase on the quenching temperature of the cast Ti–45Al–5Nb–1Mo–0.2B alloy.

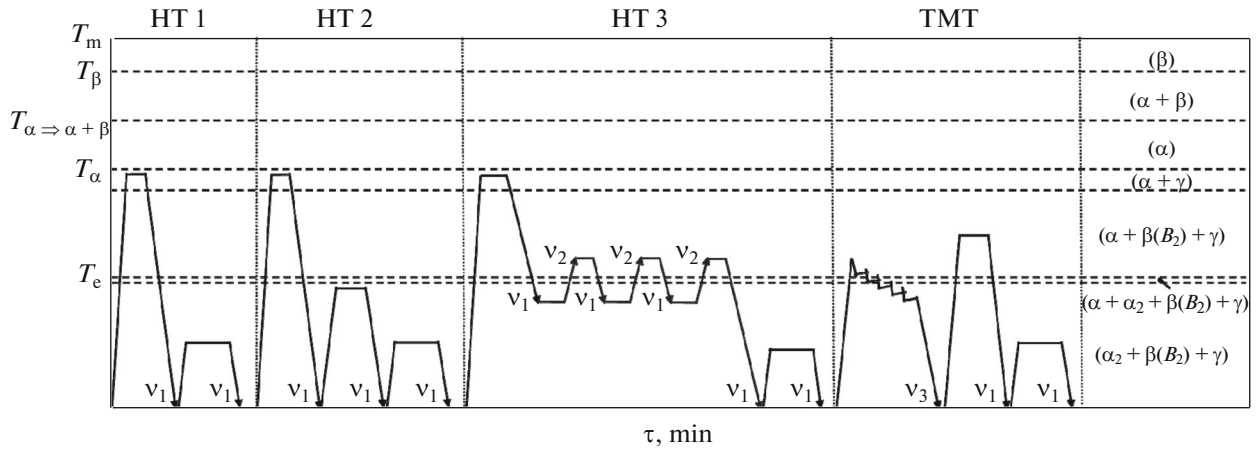

Fig. 4. Schematic diagram of heat and thermomechanical treatment conditions for the Ti–45A–5Nb–1Mo–0.2B alloy; designations ν_1, ν_2, and ν_3 correspond to furnace cooling, furnace heating, and air cooling, respectively.

Effect of Heat and Thermomechanical Treatment on the Microstructure

Figure 4 shows the scheme of heat and thermomechanical treatments of the alloy. The heat treatments (HTs) HT 1 and HT 2 include annealing at 1300°C for 0.5 h; furnace cooling; annealing at 900°C for 4 h; and, in the case of HT 2, additional annealing at 1100°C for 2 h. The cyclic heat treatment (HT 3) includes the annealing at 1300°C for 1 h, furnace cooling, cyclic annealings at 1100°C for 1 h and 1200°C for 0.5 h, and final annealing at 900°C for 4 h. The thermomechanical treatment (TMT) includes onefold compression under quasi-isothermal conditions at temperatures close to the eutectoid temperature, subsequent annealing at 1250°C for 2 h, furnace cooling, and annealing at 900°C for 4 h (Fig. 4).

HT 1 mainly leads to the formation of the lamellar microstructure with almost equilibrium colonies (Fig. 5a). The average colony size remains close to the initial size. The lamella thickness is $\lambda = 50$–600 nm. Bright $\beta(B2)$-phase interlayers remain in the structure. The volume fraction of the $\beta(B2)$ phase is 3.7%. The additional annealing at 1100°C (HT 2), which corresponds to the three-phase ($\alpha_2 + \beta(B2) + \gamma$) region, in combination with the subsequent annealing at 900°C leads to the decrease in the content of the $\beta(B2)$ phase to 3 vol % and the appearance of γ(TiAl)-phase interlayers mainly at the boundaries of colonies (Fig. 5b). This can be explained by the development of the $\alpha_2 \rightarrow \beta(B2)$ phase transformation at colony boundaries at 1100°C and subsequent $\beta(B2) \rightarrow \gamma$ transformation at 900°C. As a result, mainly the lamellar structure with an average colony size of 50 ± 3.5 μm is formed. The lamella thickness is $\lambda = 70$–800 nm.

Figure 5c shows the microstructure formed after cyclic heat treatments (HT 3), which result in the formation of mixed lamellar-globular structure with the average colony/grain size $d = 31 \pm 8$ μm. The lamella thickness in colonies is $\lambda = 0.5$–4 μm; the volume fraction of globular γ(TiAl) grains is 19% and the volume fraction of $\beta(B2)$ phase is 1.7%.

Figure 5d shows the microstructure formed after hot deformation and subsequent heat treatment. The deformation leads to the intense development of dynamic recrystallization in the majority of the parts of deformed blank; the subsequent heat treatment results in slight grain growth and the formation of a duplex microstructure that consists of γ- and α_2-phase grains and a small volume (about 15%) of the lamellar component. The average grain/colony size is $d = 8 \pm 1$ μm and the volume fraction of the $\beta(B2)$ phase is 1.3%. The deformation was performed at temperatures that correspond to the ($\alpha(\alpha_2) + \beta(B2) + \gamma$) phase region, when the alloy contains about 10 vol % $\beta(B2)$ (Fig. 3). This determines the sufficient manufacturing plasticity and allows us to obtain the resulting fine duplex microstructure. It should be noted that the used deformation treatment is significantly simpler than the hot extrusion usually applied for TNB and TNM alloys.

Mechanical Properties

Room-temperature tensile tests were performed for the alloy subjected to HT 1, HT 2, HT 3, and TMT. It can be seen that, when passing from almost completely lamellar state (HT 1) to the state characterized by the presence of a globular component (HT 2, HT 3, and TMT), the simultaneous increase in both plasticity and strength of the alloy takes place (Fig. 6). For the states obtained after heat treatments HT 2 and HT 3, the increase is slight and related to some decrease in the colony/grain size, in part the globularization of the structure, the increase in the space between lamellas, and, what is likely, a decrease in the volume fraction of the $\beta(B2)$ phase. The transition from the lamellar and lamellar-globular structure

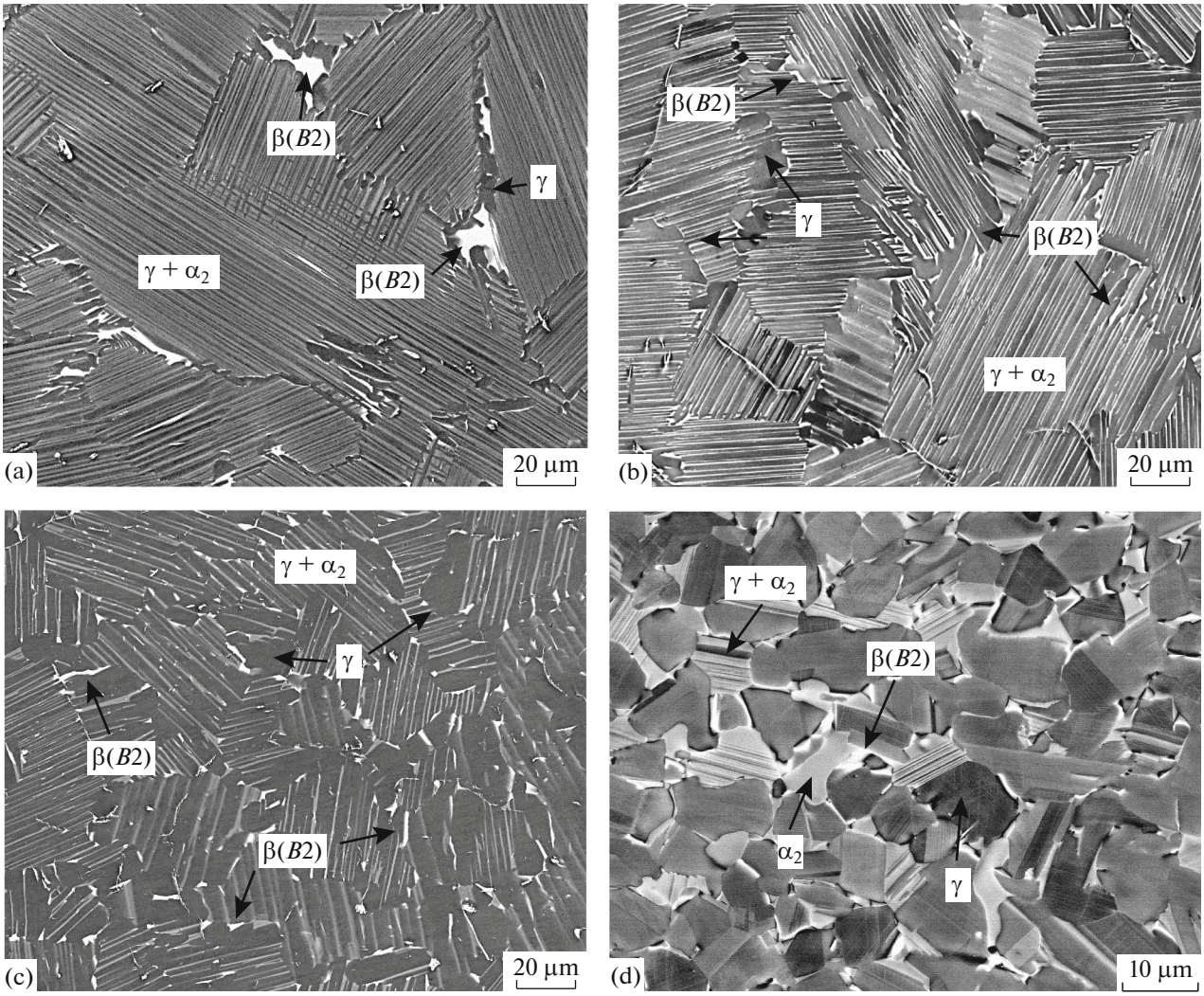

Fig. 5. Microstructure (backscattered electron mode) of the Ti–45Al–5Nb–1Mo–0.2B alloy after (a) HT 1, (b) HT 2, (c) HT 3, and (d) TMT.

(after HT 1–HT 3) to the fine duplex structure (after TMT) leads to a substantial increase in the plasticity ($\delta \approx 3.1\%$) and strength ($\sigma_u \approx 860$ MPa); this is explained first of all by the more uniform (delocalized) development of plastic deformation due to the refining of the microstructure. The possible cause for the increase in the plasticity after TMT is the fact that the grain size ($d \approx 8$ μm) is favorable for the development of deformation twining [30].

The alloy after HT 2 and TMT was subjected to fracture toughness, fatigue, and high-temperature long-term strength tests. The fracture toughness at room temperature of the sample with mainly a lamellar structure was found to be higher than that in the case of duplex structure (Table 2); this agrees with the literature data.

The fatigue strength of the with the duplex structure was found to be higher than that of a sample subjected to HT 2. No failure of the samples with the duplex structure was observed during tests at 10^7 cycles with a maximum load of 400 MPa, whereas the sample subjected to HT 2 passes only 1.67353×10^6 cycles at the maximum load of 400 MPa. At a maximum load of 370 MPa, the samples subjected to HT 2 pass 10^7 cycles without failure.

Table 2. Results of fracture toughness (K_{Ic}) and fatigue (σ_{-1}) tests at room temperature for Ti–45Al–5Nb–1Mo–0.2B alloy subjected to heat (HT 2) and thermomechanical treatment (TMT)

Treatment	K_{Ic}, MPa m$^{1/2}$	σ_{-1}, MPa $N = 10^7$ cycles
HT 2	25	>370
TMT	11	>400

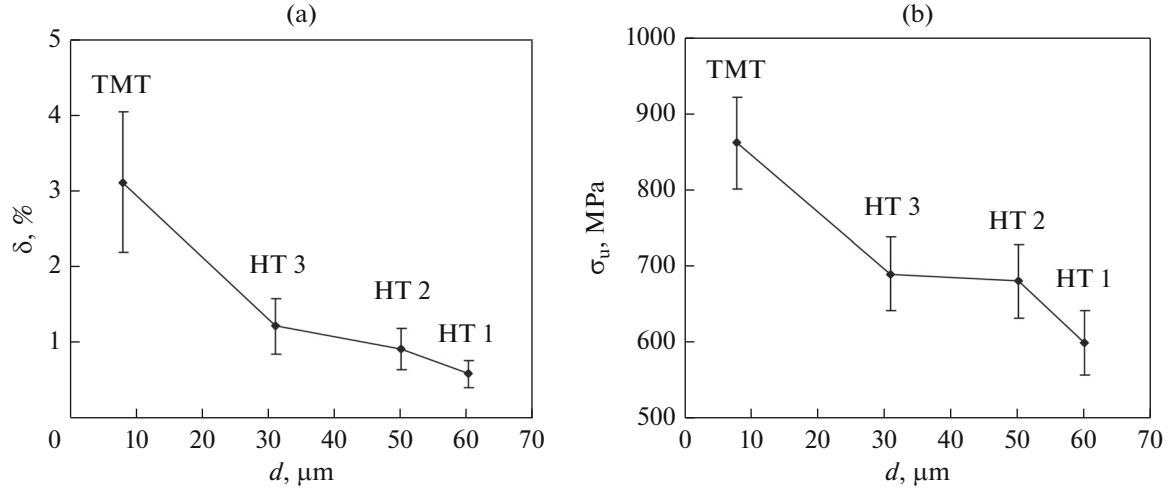

Fig. 6. Dependences of (a) relative elongation δ and (b) conventional ultimate strength σ_u on the colony/grain size d, which were determined by tensile tests of Ti–45Al–5Nb–1Mo–0.2B samples subjected to the heat and thermomechanical treatments.

A long-term strength test at 600°C and a load of 550 MPa showed that the sample with a dominant lamellar structure (after HT 2) exhibits almost no elongation, whereas the sample with the duplex structure (after TMT) demonstrates 0.6% elongation (Table 3). The long-term strength at 700–750°C of the sample with the dominating lamellar structure was found to be higher than that for the sample with the duplex structure obtained by TMT. In the case of lamellar structure, the elongation of samples at 700 and 750°C and under loads of 450 and 350 MPa was 0.8 and 3.6%, respectively. For all samples, no failure was observed during tests. Thus, we can conclude that the high density of coherent γ/γ and semicoherent γ/α_2 boundaries favors an increase in the toughness and creep resistance, whereas the fine grains/colonies in the duplex structure are favorable during fatigue tests.

A comparison of the mechanical properties of the cast Ti–45Al–5Nb–1Mo–0.2B alloy subjected to HT 2 with those of advanced cast γ(TiAl) alloys in the heat treated state shows that the reached properties are comparable with the properties of the Ti–43.7Al–3.2(Nb, Cr, Mo)–0.2B and Ti–43.5Al–4Nb–1Mo–0.1B alloys (Table 1). A comparison with the Ti–44Al–4Nb–4Hf–0.1Si–0.1B, Ti–44Al–8Nb–1B, and Ti–43Al–6Nb–1B alloys shows that the plasticity of the Ti–45Al–5Nb–1Mo–0.2B alloy is substantially higher at equal strength parameters.

Table 3. Results of long-term strength tests for the Ti–45Al–5Nb–1Mo–0.2B alloy subjected to heat (HT 2) and thermomechanical treatment (TMT)

T_{test}, °C	HT 2*		TMT*	
	P, MPa	δ, %	P, MPa	δ, %
600	550	0.05	550	0.6
700	450	0.8	350	2.3
750	350	3.6	300	17.8

* No failure of samples during tests took place.

The mechanical properties, in particular the plasticity and strength of the deformed Ti–45Al–5Nb–1Mo–0.2B alloy, exceed those of the deformed Ti–44.2Al–3(Nb, Cr, B), Ti–43Al–6Nb–1B, and Ti–44.5Al–6.25Nb–0.8Mo–0.1B alloys (Table 1). Comparison with the Ti–43.5Al–4Nb–1Mo–0.1B and Ti–45Al–8Nb–0.2C alloys shows that the plasticity of the Ti–45Al–5Nb–1Mo–0.2B alloy is slightly higher at the comparable strength parameters. Moreover, forces applied during deformation of the Ti–45Al–5Nb–1Mo–0.2B alloy by single-stage compression, the degree and forces of deformation, were found to be substantially lower than those applied during the deformation of the aforementioned alloys by extrusion and forging.

CONCLUSIONS

(1) In the initial cast state, the Ti–45Al–5Nb–1Mo–0.2B (at %) alloy is characterized by a uniform, mainly lamellar, structure with fine colonies ($d = 60 \pm 3$ μm). The following is the determined sequence of phase regions during solidification and cooling of the alloy ingot:

$$L \to L + \beta \to \beta \to \alpha + \beta \to \alpha \to \alpha + \gamma \to \alpha + \beta(B2) + \gamma \to \alpha + \alpha_2 + \beta(B2) + \gamma \to \alpha_2 + \beta(B2) + \gamma.$$

(2) The heat treatment allows us to affect the microstructure of the cast Ti–45Al–5Nb–1Mo–0.2B alloy as follows: (a) to obtain mainly a lamellar or lamellar-globular structure with interlayers and grains of the γ and β($B2$) phases along boundaries of ($\gamma + \alpha_2$) colonies; (b) to vary the thickness of lamellas; and

(c) to almost completely dissolve the β(*B*2) phase. The partial globularization of the cast structure by heat treatment allows us to slightly increase both the plasticity δ (from 0.5 to 0.9–1.2%) and strength at room temperature σ_u (600 to 670–690 MPa).

(3) The cast Ti–45Al–5Nb–1Mo–0.2B alloy that was subjected to three-stage annealing at temperatures corresponding to the (α + γ)- and (α_2 + β(*B*2) + γ) phase region and furnace cooling after each of annealings, exhibits the following mechanical properties: at room temperature, σ_u = 670 MPa, δ = 0.9%, K_{Ic} = 25 MPa $m^{1/2}$, σ_{-1} > 370 MPa for the number of cycles $N = 10^7$; at 700°C, the long-term strength is σ_{100}^{700} > 450 MPa and, at 750°C, it is σ_{100}^{750} > 350 MPa.

(4) The hot single-stage compressive deformation in an envelope at temperatures that correspond to the (α(α_2) + β(*B*2) + γ) phase region and subsequent two-stage annealing at temperatures that correspond to the (α + β(*B*2) + γ)- and (α_2 + β(*B*2) + γ) phase region leads to the formation of a fine duplex structure. This ensures the substantial increase in both plasticity and strength at room temperature and the retained high creep resistance to 700°C. The achieved state exhibits the following combination of properties at room temperature: σ_u = 860 MPa, δ = 3.1%, K_{Ic} = 11 MPa $m^{1/2}$, σ_{-1} > 400 MPa for the number of cycles $N = 10^7$; at 700°C, the long-term strength is σ_{100}^{700} > 350 MPa and, at 750°C, it is σ_{100}^{750} > 300 MPa.

ACKNOWLEDGMENTS

This study was performed in the framework of the Fundamental Research Program of the Russian Academy of Sciences, registration no. 01201455192.

REFERENCES

1. *Gamma Titanium Aluminides 2003,* Ed. by H. Kim, A. Clemens, and A. Rosenberger (TMS, Warrendale, PA, 2003).
2. *Titanium and Titanium Alloys,* Ed. by C. Leyens and P. Leyens, (Wiley-VCH, Weinheim, 2003).
3. *Structural Aluminides for Elevated Temperature Applications,* Ed. by Y.-W. Kim, D. Morris, R. Yang, and C. Leyens, (TMS, Warrendale, PA, 2008).
4. W. Smarsly, H. Baur, G. Glitz, H. Clemens, T. Khan, and M. Thomas, "Titanium aluminides for automotive and gas turbine applications," in *Structural Intermetallics,* Ed. by K. J. Hemker, D. M. Dimiduk, H. Clemens, R. Darolia, H. Inui, J. M. Larsen, K. Sikka, M. Thomas, and J. D. Whittenberger (TMS, Warrendale, PS, 2001), pp. 25–34.
5. E. N. Kablov, "Strategic directions of materials development and technologies of their treatment to 2030," Aviats. Mater. Tekhnol., No. 6, 7–17 (2012).
6. H. Clemens and S. Mayer, "Design, processing, microstructure, properties, and applications of advanced intermetallic TiAl alloys," Adv. Eng. Mater. **15**, 191–215 (2013).
7. J. M. Larsen, B. D. Worth, S. J. Balsone, and J. W. Jones, "An overview of the structural capability of available gamma titanium aluminide alloys," in *Gamma Titanium Aluminides,* Ed. by Y.-W. Kim, R. Wagner, and M. Yamaguchi (TMS, Warrendale, PA, 1995), pp. 821–834.
8. Y-W. Kim and D. M. Dimiduk, "Designing gamma TiAl alloys: Fundamentals, strategy and production," in *Structural Intermetallics*, Ed. by M. V. Nathal, E. Darolia, C. T. Liu, P. L. Martin, D. B. Miracle, R. Wagner, and M. Yamaguchi (TMS, Warrendale, PA, 1997), pp. 531–543.
9. C. M. Austin, T. J. Kelly, K. G. McAllister, and J. C. Chesnutt, "Aircraft engine applications for gamma titanium aluminide," in *Structural Intermetallics*, Ed. by M. V. Nathal, E. Darolia, C. T. Liu, P. L. Martin, D. B. Miracle, R. Wagner, and M. Yamaguchi (TMS, Warrendale, PA, 1997), pp. 413–425.
10. F. Appel, M. Oehring, and R. Wagner, "Novel design concepts for gamma-based titanium aluminide alloys," Intermetallics **8**, 1283–1312 (2000).
11. F. Appel, U. Brossmann, U. Christoph, S. Eggert, P. Janschek, U. Lorenz, J. Muellauer, M. Oehring, and J. D. H. Paul, "Recent progress in the development of gamma titanium aluminide alloys," Adv. Eng. Mater. **2**, 699–720 (2000).
12. F. Appel, U. Lorenz, J. D. H. Paul, and M. Oehring, "The mechanical properties of niobium alloyed gamma titanium aluminides," in *Gamma Titanium Aluminides*, Ed. by Y.-W. Kim, D. M. Dimiduk, and M. H. Loretto (TMS, Warrendale, PA, 1999), pp. 381–388.
13. R. Imayev, V. Imayev, M. Oehring, and F. Appel, "Alloy design concepts for refined cast and wrought gamma titanium aluminide based alloys," Intermetallics **15**, 451–460 (2007).
14. H. Clemens, W. Wallgram, S. Kremmer, V. Guther, A. Otto, and A. Bartels, "Design of novel β-solidifying TiAl alloys with adjustable β/*B*2-phase fraction and excellent hot-workability," Adv. Eng. Mater. **10**, 707–713 (2008).
15. V. M. Imayev, T. I. Oleneva, R. M. Imayev, H.-J. Christ, and H.-J. Fecht, "Microstructure and mechanical properties of low and heavy alloyed γ-TiAl+α_2-Ti_3Al based alloys subjected to different treatments," Intermetallics **26**, 91–97 (2012).
16. E. Schwaighofer, H. Clemens, S. Mayer, J. Lindemann, J. Klose, W. Smarsly, and V. Guther, "Microstructural design and mechanical properties of a cast and heat treated intermetallic multi-phase γ-TiAl based alloy," Intermetallics **44**, 128–140 (2014).
17. V. M. Imaev, R. M. Imaev, T. I. Oleneva, and T. G. Khismatullin, "Microstructure and mechanical properties of the intermetallic alloy Ti–45Al–6(Nb, Mo)–0.2B," Phys. Met. Metallogr. **106**, 641–648 (2008).
18. H. Saage, A. J. Huang, D. Hu, M. H. Loretto, and X. Wu, "Microstructures and tensile properties of massively transformed and aged Ti46Al8Nb and Ti46Al8Ta alloys," Intermetallics **17**, 32–38 (2009).

19. Z. W. Huang, W. Voice, P. Boven, T. T. Cheng, M. R. Willis, and I. P. Jones, "Effects of major alloying additions on the microstructure and mechanical properties of γ-TiAl," Intermetallics **7**, 89–99 (1999).

20. Z. W. Huang and T. Cong, "Microstructural instability and embrittlement behavior of an Al-lean, High-Nb γ-TiAl-based alloy subjected to a long-term thermal exposure in air," Intermetallics **18**, 161–172 (2010).

21. N. Z. Niu, Y. Y. Chen, F. T. Kong, and J. P. Lin, "Microstructure evolution, hot deformation behavior and mechanical properties of Ti–43Al–6Nb–1B," Intermetallics **31**, 249–256 (2012).

22. V. M. Imayev, R. M. Imayev, and A. V. Kuznetsov, "Mechanical properties of thermomechanically treated Ti-rich $\gamma + \alpha_2$ titanium aluminide alloys," Scr. Mater. **49**, 1047–1052 (2003).

23. C. T. Liu, J. H. Schneibel, P. J. Maziasz, J. L. Wright, and D. S. Easton, "Tensile properties and fracture toughness of TiAl alloys with controlled microstructures," Intermetallics **4**, 429–440 (1996).

24. F. Appel, M. Oehring, J. D. H. Paul, and U. Lorenz," Design, properties and processing of novel TiAl alloys," in *Structural Intermetallics*, Ed. by K. J. Hemker, D. D. Mimiduk, H. Clemens, R. Darolia, H. Inui, J. M. Larsen, V. K. Sikka, N. Thomas, and J. D. Whittenberger (TMS, Warrendale, PA, 2001), pp. 63–72.

25. F. Appel, M. Oehring, and J. D. H. Paul, "Nano-scale design of TiAl alloys based on β-phase decomposition," Adv. Eng. Mater. **8**, 371–376 (2006).

26. S. Bolz, M. Oehring, J. Lindemann, F. Pyczak, J. Paul, A. Stark, T. Lippmann, S. Schrufer, D. Roth-Fagaraseanu, A. Schreyer, and S. Weiß, "Microstructure and mechanical properties of a forged β-solidifying γ TiAl alloy in different heat treatment conditions," Intermetallics **58** 71–83 (2015).

27. J. D. H. Paul, U. Lorenz, M. Oehring, and F. Appel, "Up-scaling the size of TiAl components made via ingot metallurgy," Intermetallics **32**, 318–328 (2013).

28. M. Oehring, A. Stark, J. D. H. Paul, T. Lippmann, and F. Pyczak, "Microstructural refinement of boron-containing β-solidifying γ-titanium aluminide alloys through heat treatments in the β phase field," Intermetallics **32**, 12–20 (2013).

29. U. Hecht, V. Witusiewicz, A. Drevermann, and J. Zollinger, "Grain refinement by low boron additions in niobium-rich TiAl-Based Alloys," Intermetallics **16**, 969–978 (2008).

30. V. M. Imayev, R. M. Imayev, G. A. Salishchev, K. B. Povarova, M. R. Shagiev, and A. V. Kuznetsov, "Effect of grain size and strain rate on twinning and room temperature ductility of TiAl with fine equiaxed microstructure," Scr. Mater. **36**, 891–897 (1997).

Translated by N. Kol'chugina